



GCM simulations of the Indian Ocean dipole influence on East African rainfall: Present and future

D. Conway,¹ C. E. Hanson,¹ R. Doherty,² and A. Persechino^{3,4}

Received 17 July 2006; revised 15 November 2006; accepted 30 November 2006; published 9 February 2007.

[1] Six coupled GCMs are assessed in terms of their ability to simulate observed characteristics of East African rainfall, the Indian Ocean dipole and their temporal correlation. Model results are then used to analyze the future behaviour of rainfall and the DMI. All models simulate reasonably well the spatial distribution and variability of annual and seasonal rainfall over the 1961–1990 period. Model simulation of observed DMI characteristics is less consistent with observations, however, five models reproduce similar correlations to those observed between the DMI and East African short rains (SON). In the future, there are no clear inter-model patterns of rainfall or DMI behaviour. In this sample of models four (two) out of six simulate modest increases (decreases) in annual rainfall by the 2080s. For SON, three of the six models indicate a trend towards increasingly positive phase of the DMI, two indicate a decrease and one shows no substantial change. **Citation:** Conway, D., C. E. Hanson, R. Doherty, and A. Persechino (2007), GCM simulations of the Indian Ocean dipole influence on East African rainfall: Present and future, *Geophys. Res. Lett.*, 34, L03705, doi:10.1029/2006GL027597.

1. Introduction

[2] It is widely established that the Indian Ocean dipole (IOD) exerts an important influence on the behaviour of East African rainfall, perhaps even more so than the El Niño-Southern Oscillation, particularly during the short rains season of September, October and November (SON) [e.g., Black, 2005; Saji and Yamagata, 2003a; Behera et al., 2005]. Changes in rainfall in this region, under greenhouse-gas warming, are likely to have greater consequences than changes in other elements such as temperature because of the critical importance of rainfall for socio-economic activity.

[3] The strength or phase of the IOD is represented by the Dipole Mode Index (DMI), which is the sea surface temperature anomaly (SSTa) difference calculated for two regions of the Indian Ocean. The western region encompasses 50°E–70°E/10°S–10°N, and the eastern region 90°E–110°E/10°S–0°. The DMI is then the difference

between the average SSTa (calculated relative to the 1961–1990 climate normal) for the western minus the eastern region [Saji et al., 1999]. A positive phase (or a positive dipole year [Saji et al., 1999]) is associated with higher East African rainfall due to a warming of the western Indian Ocean and a cooling of the eastern Indian Ocean, leading to anomalous easterly flow of the surface winds into Africa and the advection of moist air into the region [Black et al., 2003]. A negative mode indicates more normal conditions with southeast trade winds converging into the South Equatorial Trough [Saji et al., 1999; Saji and Yamagata, 2003b].

[4] It is important that Global Climate Models (GCMs) realistically simulate East African rainfall variability across time and space, in order to provide confidence in their projections of future rainfall in this region. In addition, it is also essential that influences on rainfall behaviour on interannual timescales are also adequately modelled by GCMs. Recent GCM studies have demonstrated their ability to simulate IOD variability with varying levels of success [Cai et al., 2005; Behera et al., 2005; Spencer et al., 2005]. With this in mind, this paper aims to assess the ability of six state-of-the-art ocean-atmosphere coupled GCMs to simulate the following: the spatial and temporal characteristics of East African rainfall over the period 1961–1990 and the characteristics of, and rainfall teleconnections with, the DMI. The paper then presents projections for the future, both in terms of regional rainfall totals and DMI behaviour. The future is represented by the SRES A2 scenario which describes a world of self-reliance and preservation of local identities. This scenario has medium high emissions, with atmospheric CO₂ concentrations reaching 715 ppm and global temperatures expected to increase by around 3.3°C by the 2080s [Nakicenovic and Swart, 2000].

2. Data and Methods

[5] A high resolution (0.5° × 0.5°) data set of monthly mean and time series of gridded rainfall for land surfaces [New et al., 1999, 2000] was used to assess the ability of six GCMs to simulate rainfall for the period 1961–1990. Model data were acquired from the Programme for Climate Model Diagnosis and Inter-comparison (PCMDI website <http://www-pcmdi.llnl.gov>). The full list of GCMs investigated can be found in Table 1 with their respective spatial resolutions, developing institution, and timespan. McHugh [2005] has previously identified the CERF, ECHAM4, UKMO and UKMO3 models as accurately representing mean annual rainfall rates over East Africa. Where possible, the most up-to-date versions of these models have been included in the present study. For example, ECHAM5 replaces ECHAM4 and HadGEM1 is included as well as

¹School of Development Studies, University of East Anglia, Norwich, UK.

²Institute of Atmospheric and Environmental Science, University of Edinburgh, Edinburgh, UK.

³Tyndall Centre for Climate Change Research, School of Environmental Sciences, University of East Anglia, Norwich, UK.

⁴School of Development Studies, University of East Anglia, Norwich, UK.

Table 1. Model Name, Developing Institution, and Spatial Resolution of the Six GCMs Used in This Study

Global Climate Model	Institution	Spatial Resolution, degrees		Time Span
		Longitude	Latitude	
CCCma CGCM3.1	Canadian Centre for Climate Modelling and Analysis, Canada	3.75	3.75	1850–2100
CSIRO MK3.0	CSIRO Atmospheric Research, Australia	1.875	1.875	1871–2100
ECHAM5	Max Planck Institute for Meteorology, Germany	1.875	1.875	1860–2100
GFDL CM2.1	Geophysical Fluid Dynamics Laboratory, USA	2.5	2.0	1861–2100
HadCM3	Hadley Centre for Climate Prediction and Research, UK	3.75	2.5	1860–2099
HadGEM1	Hadley Centre for Climate Prediction and Research, UK	1.875	1.25	1860–2099

HadCM3. First, the observed and modelled data were interpolated onto a common grid resolution of 2.5° latitude \times 2.5° longitude producing an array of 14×8 grid points across the region $12.5^\circ\text{N}/20^\circ\text{S} - 25^\circ\text{E}/42.5^\circ\text{E}$ representing the whole of East Africa and parts of central and southern Africa. This region extends slightly south of the main IOD influence on East African rainfall, which is about 10°S . Modest variation in the boundaries of the region for short rains in East Africa does not affect the results to any great degree. Then, in order to assess the ability of the models to simulate the observed climatological mean annual and seasonal rainfall distribution for the 1961–1990 period, field correlations were calculated. Normalized root mean squared errors (NRMSE) were also calculated between model and observations in order to assess the ability of the models to simulate realistic, observed variability. Here, the root mean square errors were normalised by the standard deviation of the observed values. Where NRMSE values are close to 1.0 this indicates the models are performing within the range of that observed [see *McHugh*, 2005]. Field correlations ≥ 0.60 and NRMSE of between 0.8–1.2 were chosen to identify which GCMs accurately simulate annual and seasonal rainfall characteristics across East Africa.

[6] The Indian Ocean DMI was calculated for each model at annual and seasonal scales. The observed and model DMI were calculated using the method described in section one. The HadISST data set for the period 1870–2003 was used to calculate the observed DMI, GCM SSTs were used to calculate model DMIs for the time periods shown in Table 1, and surface air temperatures (2 m) were used for EOF analysis to characterise the centres of dipole activity (section 3.1.).

3. Results

3.1. GCM Simulation of Observed Rainfall, the DMI, and Their Association

[7] Table 2 shows that ECHAM5 and HadGEM1 models produced consistently high field correlations for rainfall in all seasons over the 1961–90 period. The other models produce lower field correlations for the long rains season (March–May, MAM). Five models produce annual NRMSE from 0.8–1.2, but produce DJF and JJA (dry seasons) NRMSE below 0.8. Plots of annual observed and simulated rainfall (not shown) show good agreement for CSIRO and GFDL, ECHAM5 is too dry whilst the other models are too wet. Plots of observed and simulated SON rainfall (Figure 1) show larger proportional errors, except for ECHAM5. All the models except ECHAM5 are markedly too wet.

[8] EOF analysis of Indian Ocean surface air temperatures simulated by the six climate models shows good correspondence between the observed EOF patterns and

those in the models (not shown). Five out of six models simulate an east-west dipole pattern in the second EOF mode (EOF2; EOF1 represents a basin-wide pattern related to ENSO), similar to EOF2 in the observations. The CSIRO GCM simulates a dipole pattern in EOF3. The centres of dipole activity generally occur in similar locations to those in the observations and those used to define the DMI, although some of the models exhibit dipole centres extending slightly south of the observations. The boxes commonly used to define the DMI in the observations (section 2) are therefore used here to generate DMIs from the GCMs as they capture the core and peripheral areas of dipole activity in the west and east Indian Ocean reasonably well.

[9] Figure 2 shows time series of observed and modelled DMI for the SON season. Two (two) models show a marked (moderate) positive bias in SON DMI and five show greater variability. Table 3 lists the area average SSTs for the west and east Indian Ocean boxes and their absolute difference (west minus east). CCCma has a warm SST bias in the west

Table 2. Field Correlations and NRMSE Between Observed and GCM Rainfall for Each Model and Season, Average Over the 1961–1990 Climate Normal^a

Model	Season	Correlation	NRMSE
CCCma CGCM3.1	Annual	0.66	1.28
	<i>DJF</i>	0.67	0.89
	MAM	0.47	1.11
	JJA	0.88	0.77
	SON	0.85	1.49
CSIRO MK3.0	<i>Annual</i>	0.65	0.98
	DJF	0.79	0.63
	MAM	0.41	1.04
	JJA	0.89	0.51
	SON	0.81	1.09
ECHAM5	<i>Annual</i>	0.72	0.83
	DJF	0.80	0.60
	MAM	0.62	0.92
	JJA	0.90	0.56
GFDL CM2.1	SON	0.80	0.81
	Annual	0.59	0.86
	DJF	0.80	0.63
	MAM	0.45	0.96
	JJA	0.80	0.66
HadCM3	SON	0.75	0.84
	<i>Annual</i>	0.69	0.97
	DJF	0.75	0.67
	MAM	0.46	0.14
HadGEM1	JJA	0.85	0.55
	SON	0.84	0.94
	<i>Annual</i>	0.68	0.90
	DJF	0.83	0.63
	MAM	0.60	0.89
HadGEM1	JJA	0.97	0.53
	SON	0.75	1.28

^aItalicized entries indicate field correlations ≥ 0.6 and/or NRMSE between 0.8–1.2.

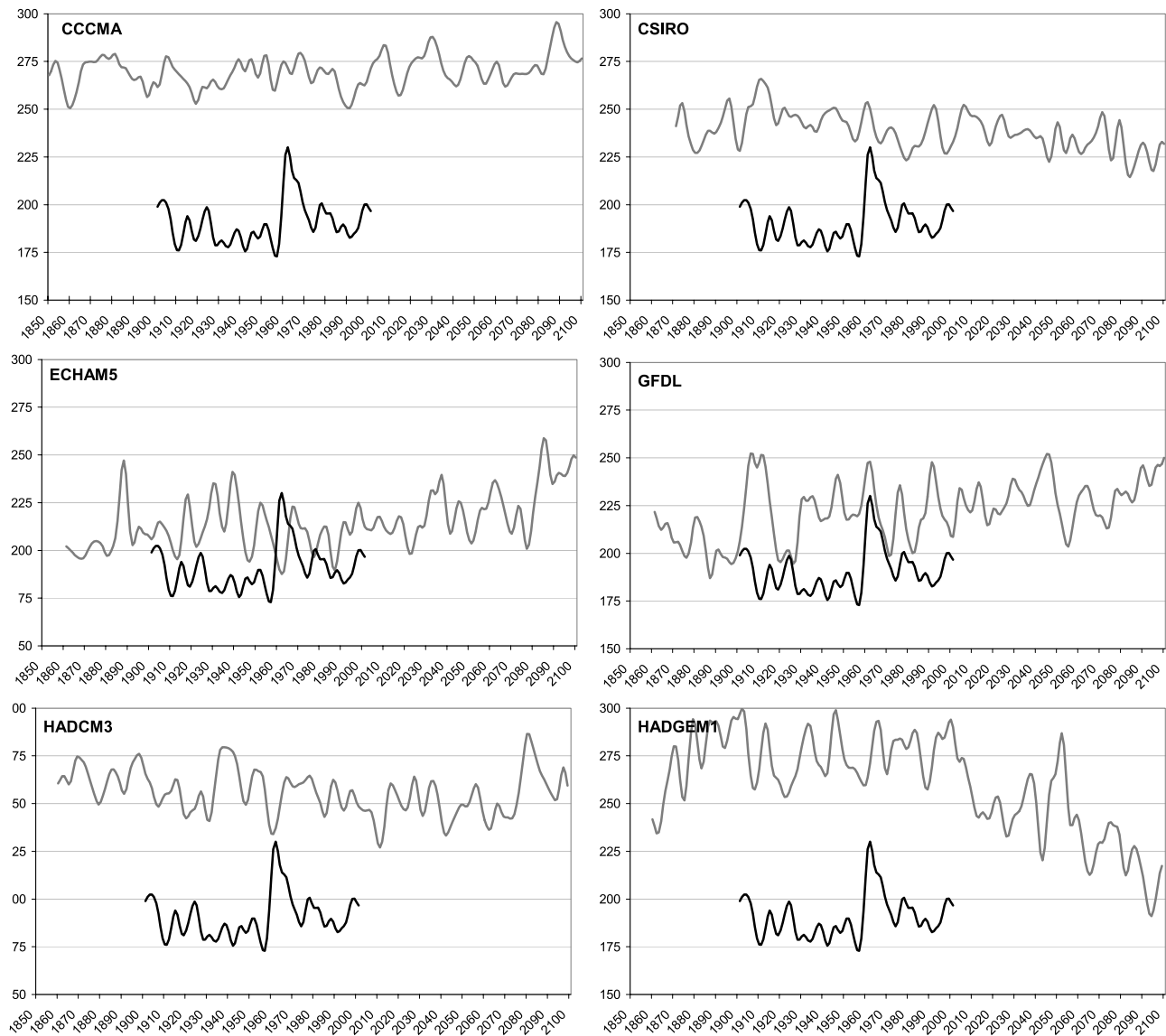


Figure 1. Observed (black, 1901–2000) and modelled (grey, ~1850s–2100) seasonal (SON) rainfall totals. The data are smoothed using an 11-point Gaussian filter.

Indian Ocean but the other models show similar patterns to the observations, except HadCM3 (too large temperature difference) and HadGEM1 (too small). With the exception of GFDL none of the models simulate the positive tendency of the SON DMI found in the observed record most notably from the mid-1970s.

[10] The models were examined in terms of their ability to simulate the positive correlations found in the observations between SON rainfall and DMI. As discussed earlier, it is well established that the IOD typically exerts its strongest influence on East African rainfall during SON. Table 4 shows the mean, minimum and maximum correlation coefficients between rainfall and the DMI from a 30-year sliding window for ~1850–2000. Five models reproduce the observed positive correlation between the DMI and SON rainfall, four are significant to the 5% level, and one model and the observations are significant to the 1% level. Two (three) models also produce spurious correlations with DJF (annual) rainfall. Temporal instability in the observed

DMI rainfall association is demonstrated by the wide range between minimum and maximum correlations. All the models exhibit temporal instability of equal and slightly larger proportions than the observations and in some cases the association breaks down completely.

3.2. GCM Simulation of Future Rainfall

[11] As illustrated in Figure 1, with this sample of models there are no clear multi-model patterns of future trends in annual rainfall change even by the 2080s; two models produce increases, two produce decreases and two produce stable regimes. All the changes are fairly modest relative to observed levels of decadal variability. Per cent changes in 30-year mean annual rainfall from 1961–1990 to 2021–2050 (2030s) are all less than 5%, with three models increasing and three decreasing (Table 5). By the 2080s the changes are larger, although still within ± 10 per cent, with two models producing a different direction of change to that in the 2030s and four of the six producing increases in rainfall. Seasonal changes are generally larger, and tend

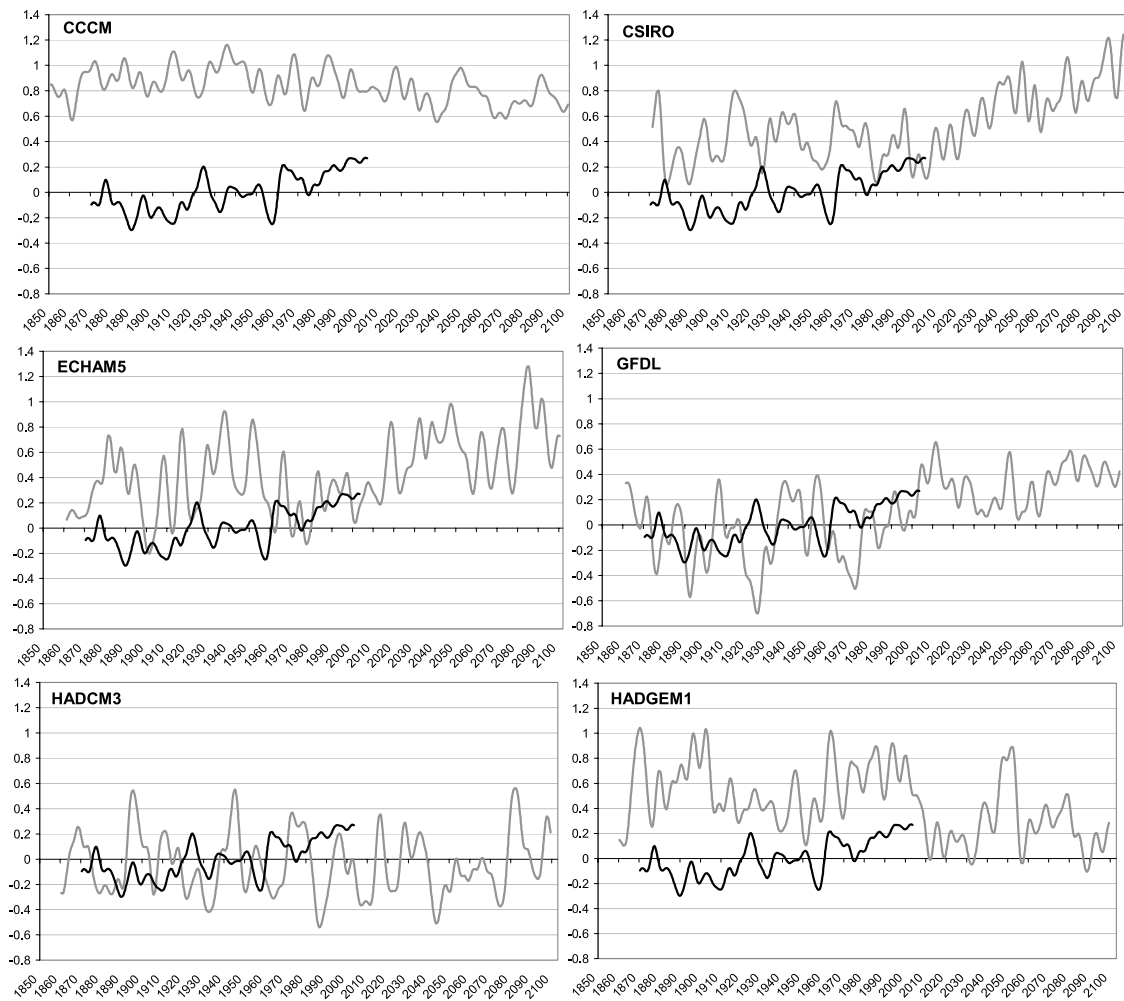


Figure 2. Observed (black, 1870–2003) and modelled (grey, ~1850s–2100) seasonal (SON) DMI. The data are smoothed using an 11-point Gaussian filter.

to be positive in SON (both periods, four out of six models) and DJF (both periods, five out of six models). The long rains season tends to decrease in both periods in five and four of the six models for the 2030s and 2080s, respectively.

3.3. GCM Simulation of Future SON DMI and Its Association With Rainfall

[12] For the DMI two models, ECHAM5 and CSIRO, produce an increasingly positive DMI as a fairly even trend in the future (Figure 2). Of the remaining models, HadCM3 and GFDL indicate no marked trend in the DMI throughout

the 21st century. HadGEM1 and CCCma show a tendency towards the negative phase of the DMI, manifest as a step-like drop by HadGEM1 and more of a steady, slight trend by CCCma (Figure 2). Changes in SSTs for the future (Table 3) show greater warming in the western sector relative to the eastern sector of the Indian Ocean, leading to a reversal in the temperature difference with CSIRO, ECHAM5 and GFDL. CCCma and HadCM3 display similar warming rates in the eastern and western sectors, whilst

Table 3. SST Area Averages in SON for West (W) and East (E) and West Minus East (W–E) Indian Ocean in °C^a

Model	1961–90	2030s			2080s		
	SST W–E	SST W–E	SST Δ East	SST Δ West	SST W–E	SST Δ East	SST Δ West
CCCma	1.15	0.99	1.44	1.28	0.97	3.09	2.91
CSIRO	–0.32	0.07	0.59	0.98	0.28	1.69	2.28
ECHAM5	–0.30	0.15	0.57	1.03	0.30	2.57	3.18
GFDL	–0.44	–0.11	0.91	1.24	0.11	2.33	2.89
HadCM3	–0.98	–0.99	0.93	0.92	–0.82	2.39	2.54
HadGEM1	–0.04	–0.41	1.33	0.96	–0.51	3.23	2.76
Observations	–0.50	–	–	–	–	–	–

^aChanges in temperature (future minus current) shown between 1961–90 and the 2030s and 2080s.

Table 4. Mean, Minimum and Maximum^a of 30-Year Running Correlations Between Rainfall and DMI for ~1850–2000 and 2001–2100^b

	~1850–2000			2001–2100		
	DJF	SON	ANNUAL	DJF	SON	ANNUAL
CCCma CGCM3.1	<i>0.408</i>	<i>0.413</i>	0.320	0.228	0.312	0.306
	0.651	0.645	0.649	0.487	0.606	0.662
	0.109	0.153	0.036	–0.290	0.053	–0.064
CSIRO MK3.0	0.239	<i>0.409</i>	0.292	0.308	0.519	0.264
	0.490	0.593	0.468	0.572	0.654	0.441
	–0.011	0.200	0.042	–0.054	0.400	–0.104
ECHAM5	0.019	0.216	0.586	0.205	0.685	0.122
	0.392	0.414	0.774	0.418	0.824	0.391
	–0.240	–0.087	0.363	0.024	0.445	–0.104
GFDL CM2.1	0.513	<i>0.410</i>	0.252	0.103	0.289	0.167
	0.806	0.827	0.635	0.416	0.543	0.371
	0.082	0.071	–0.010	–0.135	0.038	–0.069
HadCM3	0.245	<i>0.419</i>	<i>0.430</i>	0.334	0.588	0.609
	0.566	0.625	0.686	0.520	0.772	0.812
	–0.052	0.113	0.041	0.121	0.355	0.377
HadGEM1	0.306	0.562	0.499	0.035	0.662	0.283
	0.494	0.728	0.669	0.362	0.823	0.613
	–0.083	0.246	0.161	–0.659	0.462	–0.099
Observations	0.072	0.549	0.272			
	0.376	0.762	0.533			
	–0.150	0.211	–0.046			

^aMean (top), maximum (middle), and minimum (bottom). Values in bold are significant at the 0.01 level, italics significant at the 0.05 level, significance levels not shown for minimum and maximum correlations.

^bValues in bold are significant at the 0.01 level, italics significant at the 0.05 level, significance levels not shown for minimum and maximum correlations.

HadGEM1 warms faster in the east, enhancing the east-west temperature difference.

[13] Table 4 shows the mean, minimum and maximum correlations between rainfall and DMI from a 30-year sliding window for 2001–2100. The mean correlations for the future increase with CSIRO, ECHAM5, HadCM3 and HadGEM1 and decrease with CCCma and GFDL. The increase is substantial in ECHAM5 and the minimum and maximum correlations also increase in most cases. Seasonal changes in DMI are not always associated with changes in rainfall that are consistent with the observed and simulated positive relationship. For example, SON DMI increases and rainfall decreases slightly in CSIRO, despite a significant positive correlation between the two. Similar, but smaller, changes occur in CCCma but are reflected by a decrease in the correlation between the DMI and rainfall. HadGEM1, ECHAM5 and, to a lesser extent GFDL, show consistent changes, with positive DMI associated with increasing rainfall. This is an interesting area for further analysis; to gain a better understanding of the interaction between the IOD and other, potentially confounding, influences on SON rainfall in East Africa and their response to greenhouse gas forcing.

4. Discussion and Conclusions

[14] Six ocean-atmosphere coupled GCMs have been assessed in terms of their ability to simulate the characteristics of (1) observed rainfall in East Africa and (2) the behaviour of the Indian Ocean dipole (DMI) and its association with East African rainfall. The future behaviour of rainfall and the DMI have been presented in response to climate change due to the SRES A2 emissions scenario. Particular attention was given to the SON season because it

exhibits the main association between rainfall and the DMI, and it contributes significantly to total annual rainfall. Occasional highly positive IOD years (e.g., 1961 and 1997) are associated with extreme SON rainfall seasons that cause major socio-economic impacts [Conway, 2002].

[15] The models generally all reveal consistently high field correlations based on the annual and seasonal distribution of rainfall across East Africa but five are too wet. Five models simulate the observed correlation between SON DMI and rainfall, although slightly weaker than in the observations, and one model has a reversed west-east Indian Ocean temperature gradient.

[16] For the future, the models show conflicting patterns of behaviour in the DMI in SON. Three of the six models

Table 5. Percent Changes in Model Rainfall for Two Periods in the Future, 2030s and 2080s

	DJF	Season/Annual			
		MAM	JJA	SON	Annual
1961–90/2021–50					
CCCma CGCM3.1	+3.1	+5.3	–1.0	+1.9	+2.6
CSIRO MK3.0	+2.4	–1.9	–1.8	+1.3	+0.4
ECHAM5	+4.7	–3.2	+0.9	+6.9	+2.8
GFDL CM2.1	0	–4.2	–4.3	+6.9	–0.2
HadCM3	+3.8	–0.7	–3.7	–2.7	–0.5
HadGEM1	–3.8	–0.9	–4.1	–11.2	–4.9
1961–90/2071–2100					
CCCma CGCM3.1	+8.0	+11.0	–3.6	+3.4	+6.1
CSIRO MK3.0	+4.1	–6.1	–2.5	–2.1	–0.7
ECHAM5	+9.1	+3.2	+4.6	+14.2	+9.3
GFDL CM2.1	+3.7	–3.8	–12.1	+6.9	+1.2
HadCM3	+7.4	–1.9	+0.5	+2.3	+3.1
HadGEM1	–2.9	–4.1	+0.5	–21.2	–6.5

indicate a trend towards an increasingly positive phase, two indicate a decrease and one shows no substantial change. Annual changes in rainfall are modest by the 2030s and 2080s, with a tendency for drying in MAM to be slightly offset by wetting in SON to produce overall changes in annual rainfall within 10% of the current mean conditions. These changes are consistent with other reviews of climate model rainfall projections in East Africa, which suggest a trend towards slightly wetter conditions with a moderate level of inter-model differences [Hulme *et al.*, 2001; McHugh, 2005].

[17] Our results demonstrate that with this sample of models no clear signal emerges in the future behaviour of SON DMI and East African rainfall. We find that models simulate differing responses in Indian Ocean SST patterns to greenhouse gas forcing with varying consequences for future DMI behaviour. This uncertainty is compounded by instability in the association between the DMI and East African rainfall and its likely interaction with changes in other influences that have not been considered here. Further detailed analysis of the realism of model simulations of the IOD, the temporal instability of its teleconnections and its response to greenhouse gas forcing is required, before we can support a more robust conclusion about future rainfall conditions in East Africa.

[18] **Acknowledgments.** The authors would like to thank Emily Black and Hilary Spencer for providing the observed DMI. We acknowledge the modelling groups for providing their data for analysis, the Program for Climate Model Diagnosis and Intercomparison (PCMDI) for collecting and archiving the model output, and the JSC/CLIVAR Working Group on Coupled Modelling (WGCM) for organizing the model data analysis activity. The multi-model data archive is supported by the Office of Science, U.S. Department of Energy. This research has been funded as part of the National Science Foundation Biocomplexity of Coupled Human and Natural Systems Program, Award BCS 0308420, and Michigan State University, USA. We thank Simon Busby for preparing EOF analyses and two anonymous reviewers for helpful comments on an earlier version of this paper.

References

- Behera, S. K., J. J. Luo, S. Masson, T. Yamagata, P. Delecluse, S. Gualdi, and A. Navarra (2005), Paramount impact of the Indian Ocean dipole on the East African short rains: A CGCM study, *J. Clim.*, *18*, 4514–4530.
- Black, E. (2005), The relationship between Indian Ocean sea-surface temperature and East African rainfall, *Philos. Trans. R. Soc., Ser. A*, *363*, 43–47.
- Black, E., J. Slingo, and K. R. Sperber (2003), An observational study of the relationship between excessively strong short rains in coastal East Africa and Indian Ocean SST, *Mon. Weather Rev.*, *131*, 74–94.
- Cai, W., H. H. Hendon, and G. Meyers (2005), Indian Ocean dipole-like variability in the CSIRO Mark 3 coupled climate model, *J. Clim.*, *18*, 1449–1468.
- Conway, D. (2002), Extreme rainfall events and lake level changes in East Africa: Recent events and historical precedents, in *The East African Great Lakes: Limnology, Palaeolimnology and Biodiversity*, *Adv. Global Change Res.*, vol. 12, edited by E. O. Odada and D. O. Olago, pp. 63–92, Springer, New York.
- Hulme, M., R. Doherty, T. Ngara, M. New, and D. Lister (2001), African climate change: 1900–2100, *Clim. Res.*, *17*, 145–168.
- McHugh, M. J. (2005), Multi-model trends in East African rainfall associated with increased CO₂, *Geophys. Res. Lett.*, *32*, L01707, doi:10.1029/2004GL021632.
- Nakicenovic, N., and R. Swart (Eds.) (2000), *Special Report on Emissions Scenarios*, Cambridge Univ. Press, New York.
- New, M. G., M. Hulme, and P. D. Jones (1999), Representing twentieth century space-time climate variability: Part I. Development of 1961–1990 mean monthly terrestrial climatology, *J. Clim.*, *12*, 829–856.
- New, M. G., M. Hulme, and P. D. Jones (2000), Representing twentieth century space-time climate variability: Part II. Development of 1901–1996 monthly grids of terrestrial surface climate, *J. Clim.*, *13*, 2217–2238.
- Saji, N. H., and T. Yamagata (2003a), Structure of SST and surface wind variability during Indian Ocean dipole mode events: COADS observations, *J. Clim.*, *16*, 2735–2751.
- Saji, N. H., and T. Yamagata (2003b), Possible impacts of Indian Ocean dipole mode events on global climate, *Clim. Res.*, *25*, 151–169.
- Saji, N. H., B. N. Goswami, P. N. Vinayachandran, and T. Yamagata (1999), A dipole mode in the tropical Indian Ocean, *Nature*, *401*, 360–363.
- Spencer, H., R. T. Sutton, J. M. Slingo, M. Roberts, and E. Black (2005), Indian Ocean climate and dipole variability in Hadley Centre coupled GCMs, *J. Clim.*, *18*, 2286–2307.

 D. Conway and C. E. Hanson, School of Development Studies, University of East Anglia, Norwich NR4 6JL, UK. (d.conway@uea.ac.uk)
 R. Doherty, Institute of Atmospheric and Environmental Science, Crew Building, University of Edinburgh, King's Buildings, Edinburgh EH9 3JN, UK.
 A. Persechini, Tyndall Centre for Climate Change Research, University of East Anglia, Norwich NR4 6JL, UK.